Observations of FeO Reduction in Electric Arc Furnace Slag by Aluminum Black Dross: Effect of CaO Fluxing on Slag Morphology

JUNG HO HEO, TAE SUNG KIM, VEENA SAHAJWALLA, and JOO HYUN PARK

The effect of CaO fluxing on slag morphology was investigated during the reduction of FeO in electric arc furnace slag by aluminum black dross (ABD). Macro- and microscopic observations, by evaluating entrapped gas bubbles and reduced iron droplets related to gas evolution, apparent slag morphologies, and vertical section of slag at different initial CaO contents and reaction times, confirmed that both aluminothermic (dominant reaction) and carbothermic (minor) reduction occurred. Thus, the production of $CO(+CO_2)$ gas caused swelling-shrinking phenomena with repeated expansion and collapse of the slag pellet. In addition, macroscopic observation of slag morphologies as a function of the initial CaO content is well associated with quantitative consideration of the apparent viscosity as well as spinel ($[Mg,Fe]Al_2O_4$) activity. Consequently, appropriate CaO fluxing is necessary to control the composition of highly fluid slag by changing the slag from a high-alumina system to calcium–aluminosilicate melts when utilizing ABD as a reducing agent.

I. INTRODUCTION

ALUMINUM dross by-products of the aluminum industry are typically classified into three types based on their concentrations of metallic Al: aluminum white dross (AWD, 15-70 mass pct Al), aluminum black dross (ABD, 10-20 pct Al), and aluminum salt cake (ASC, approximately 5 pct Al).[1,2] In particular, ABD is classified as hazardous waste according to the European Waste Catalogue and the United States Environmental Protection Agency's Hazardous Waste List (entry 100309), because ABD has the following listed properties: highly flammable (H3-A), harmful (H5), toxic (H6), leachable (H13), and ecotoxic (H14).[3] ABD reacts strongly with water, leaching out harmful and toxic gases such as NH_3, CH_4, PH_3, and H_2S.[2,4] Thus, several physicochemical studies on the characterization of ABD have been carried out, including investigations of properties such as density,[5,6] porosity,[6] and toxicity[1] as well as mineralogical and structural interpretations.[7–11]

Hydrolysis treatment of Al dross to convert it to a non-hazardous material has been experimentally investigated.[12] Nonetheless, ABD has been indiscriminately discarded in landfills or disposed of without appropriate treatment, thus contaminating the environment by introducing undesirable species such as F^-, Cl^-, NH_4^+, and CN^- into groundwater and toxic gases into the atmosphere.[2] Similarly, electric arc furnace (EAF) slag, which is also categorized as a hazardous waste in the steelmaking industry according to the list mentioned above (entry 100201),[3] has generally been disposed of in landfills.[13] Landfilling of EAF slag is problematic because of its environmental contamination by means of leaching, which can lead to many physical disorders and health concerns. Furthermore, the generation of huge amounts of EAF slag causes waste management difficulties, quickly filling landfill sites. Hence, it is very important to develop efficient solutions to manage ABD and EAF slag.

One well-known solution is to utilize ABD and EAF slag directly as raw materials as substitutes for concrete and ceramics in the fields of building and road construction. Slags have good properties for this purpose, such as corrosion and thermal shock resistance, refractoriness, and abrasion resistance. In addition, several investigations have been made into the application of ABD as an Al_2O_3 source for Al_2O_3-containing refractory bricks and cements.[10,14,15] Similarly, several

JUNG HO HEO is with the Research & Development Center, LS-Nikko Copper Inc., Ulsan 44997, Korea. TAE SUNG KIM is with the Department of Materials Engineering, Hanyang University, Ansan 15588, Korea. VEENA SAHAJWALLA is with the Centre for Sustainable Materials Research and Technology (SMaRT) of the School of Materials Science and Engineering, University of New South Wales, Sydney, NSW 2052, Australia. JOO HYUN PARK is with the Department of Materials Engineering, Hanyang University, and also with the Department of Materials Science and Engineering, KTH Royal Institute of Technology, Stockholm 100 44, Sweden.

researchers have investigated some applications of EAF slag as supplementary cementitious materials, similar to the present use of blast furnace (BF) slag.[16–18] Even though these applications have practical advantages, the challenge of managing ABD and EAF slag remains an important goal.

One possible approach to solve the problems mentioned above is to recover valuable metals such as aluminum from ABD and iron and/or manganese from EAF slag.[1,2,6,11,19–24] Thus, various researchers have attempted to recover metallic Al, Mn, and Fe by means of various physicochemical processing methods. Similarly, we have investigated the reduction behavior of FeO (and MnO) and Fe (and Mn) recovery from EAF slag by using ABD, which was used as a reducing agent because of its high reactivity, namely in aluminothermic smelting reduction (ASR).[23,24] Specifically, it was experimentally confirmed that adding a proper amount of CaO into EAF slag is efficient in the recovery of iron and manganese from EAF slag by ABD, with high yield up to about 90 pct. This is because CaO in molten EAF slag increases the slag's fluidity, which is a key factor for high recovery of iron and manganese from the molten slag.

Even though the viscosity of molten slag during the reduction reaction was quantitatively evaluated, macroscopic observations have yet not been attempted to confirm how strongly the system is affected by slag viscosity. Therefore, as a follow-up to previous research,[24] in the present work, we investigated the effect of CaO fluxing upon slag morphology during the reduction of FeO in EAF slag by ABD by *in-situ* observation of differences in pellet shape. This study will macroscopically confirm the importance of appropriate CaO fluxing of EAF slag when ABD is used as a reducing agent.

II. EXPERIMENTAL PROCEDURE

Industrial EAF slag and ABD (supplied by a domestic steel company) and reagent-grade CaO were finely crushed using a stainless steel mortar and then sieved to ensure homogeneous particles < 100 μm. The CaO was prepared by calcining $CaCO_3$ in a muffle furnace at 1273 K (1000 °C) for 10 hours under ambient atmosphere. The compositions of the EAF slag and ABD used in the present study are listed in Table I. The experimental conditions of 25.7, 38.2, and 47.0 mass pct initial CaO content are respectively equivalent to the additions of 0, 20, and 40 g CaO in previous research.[24]

All samples were homogeneously mixed, and the samples were cylindrically pelletized (diameter: 10 mm; height: 5 mm) using a stainless steel mold under 100 bar of pressure for 5 minutes. Reaction phenomena were investigated during experiments in a horizontal tube furnace at 1773 K (1500 °C), controlled within ± 2 K using a proportional integral differential controller. The horizontal tube furnace, provided by the Centre for Sustainable Materials Research and Technology (SMaRT Centre), University of New South Wales, is illustrated schematically in Figure 1.

High-purity Ar gas flowed continuously at a rate of 1 L/min using a ball flow meter during the experiment to maintain an inert atmosphere. A pellet sample was placed on the silica substrate at the tip of a graphite holder connected to a graphite rod. After purging the furnace with inert gas for 10 minutes, the assembly was first inserted into the cold zone, which was about 573 K (300 °C), at the corner of the furnace tube for about 5 minutes to prevent thermal shock to the graphite holder. The assembly was then carefully inserted into the hot zone of the furnace.

The experimental times were 1, 3, 5, and 10 minutes. The reaction phenomena were recorded onto a DVD using a CCD camera, and gas compositions were confirmed using a gas analyzer during the experiments. After the experiment, each sample was carefully vertically cross-sectioned at its center. One half was prepared by cold mounting with epoxy resin and slightly polishing the surface of the sample for observation using scanning electron microscopy equipped with energy-dispersive spectroscopy (SEM-EDS, MIRA 3, TESCAN Ltd.), and the other was carefully separated from the substrate and finely crushed into fine powder for X-ray fluoroscopy (XRF, ZSX Primus II, Rigaku) analysis. Finally, images of the pellets were extracted from the recorder.

III. RESULTS AND DISCUSSION

A. Macroscopic Observations of Slag Morphologies at Different Initial CaO Contents at Various Reaction Times

The shape changes of pellets *vs*. the initial CaO content after various reaction times at 1773 K (1500 °C) are shown in Figure 2. In an initial stage at 1 minute, the surfaces of the pellets were slightly swollen irrespective of their initial CaO content because the pellet surface was first affected by heat flow from the surroundings, leading to the following aluminothermic reaction between the FeO in the EAF slag and the Al in the ABD.[25]

$$2Al(l) + 3(FeO) = (Al_2O_3) + 3Fe(l),$$
$$\Delta G° = -919,500 + 166\ T(J/mol). \quad [1]$$
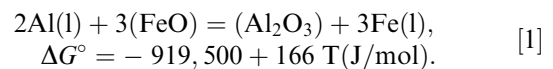
With progressive reaction times, we experimentally observed that the pellets repeatedly expanded and collapsed, except for *Sample C* ([CaO]$_{initial}$ = 47.0 pct), which fully melted after 5 minutes, although it showed the same phenomena before melting. This was due to CO and/or CO_2 gas evolution owing to carbothermic reduction between FeO in the EAF slag and carbide in the ABD.

Even though various researchers have reported the presence of aluminum carbide (Al_4C_3) in Al dross,[5,7,8] the thermodynamic assessment for the stable form of carbide in ABD is needed. Hence, the phase stability diagram of ABD at 1773 K (1500 °C) was computed using FactSage™7.3 software, as shown in Figure 3. Various carbide phases such as Al_4C_3, SiC, and Al_4C_4Si are possible according to the C and Al concentration,

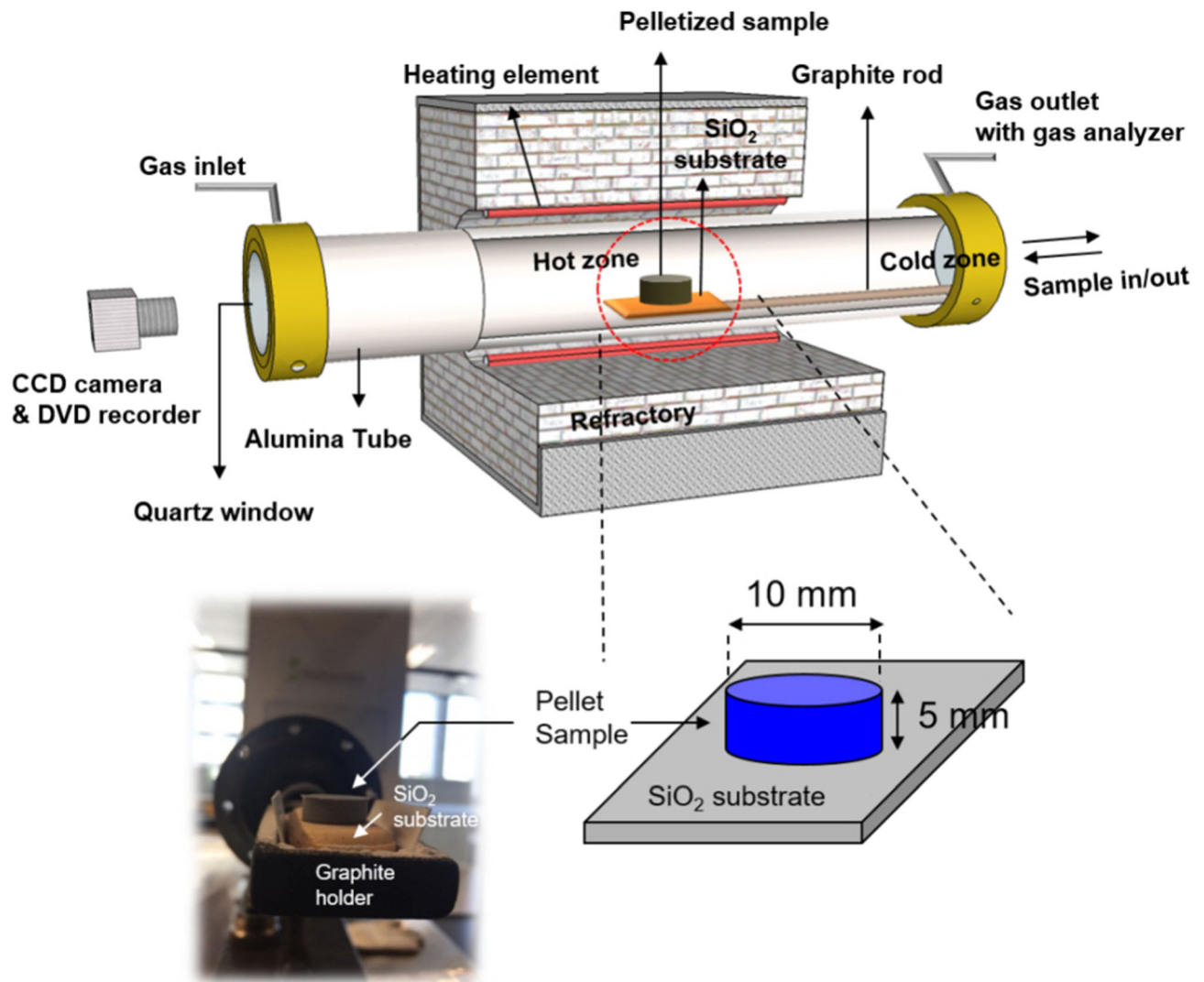|	Tot. Al	Met. Al	Al_2O_3	FeO	SiO_2	MgO	MnO	CaO	P_2O_5	S	C
EAF Slag	—	—	15.6	19.9	23.0	9.5	6.1	25.7	0.15	—	—
ABD	49.7	19.4	—	1.2	6.0	6.7	0.2	1.5	—	0.2	1.1

Fig. 1—Schematic diagram of the experimental apparatus.

and the stable carbide is clearly confirmed to be Al_4C_3 in the present ABD condition. Moreover, the Gibbs free energy of the formation reaction of Al_4C_3 at 1773 K (1500 °C) is also strongly negative (~ 96 kJ/mol) based on the following equation[25]

$$4Al(l) + 3C(s) = Al_4C_3(s),$$
$$\Delta G^{\circ} = -265,099 + 95.11T(J/mol). \qquad [2]$$
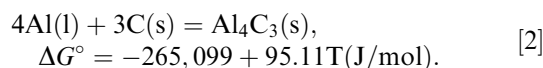
Although we could not identify the Al_4C_3 phase in ABD by XRD analysis because of the relatively small amount of carbon (1.1 mass pct, Table I) in ABD, it is reasonable to assume that the Al_4C_3 used in the present study is a stable carbide in ABD. Hence, it is believed that the FeO reduction reaction by Al_4C_3 occurs based on Eq. [3]. Furthermore, an indirect reduction of FeO by CO gas is also expressed in Eq. [4].[25]

(a) Sample A; (CaO)ᵢ= 25.7 pct, No CaO addition

(b) Sample B; (CaO)ᵢ= 38.2 pct
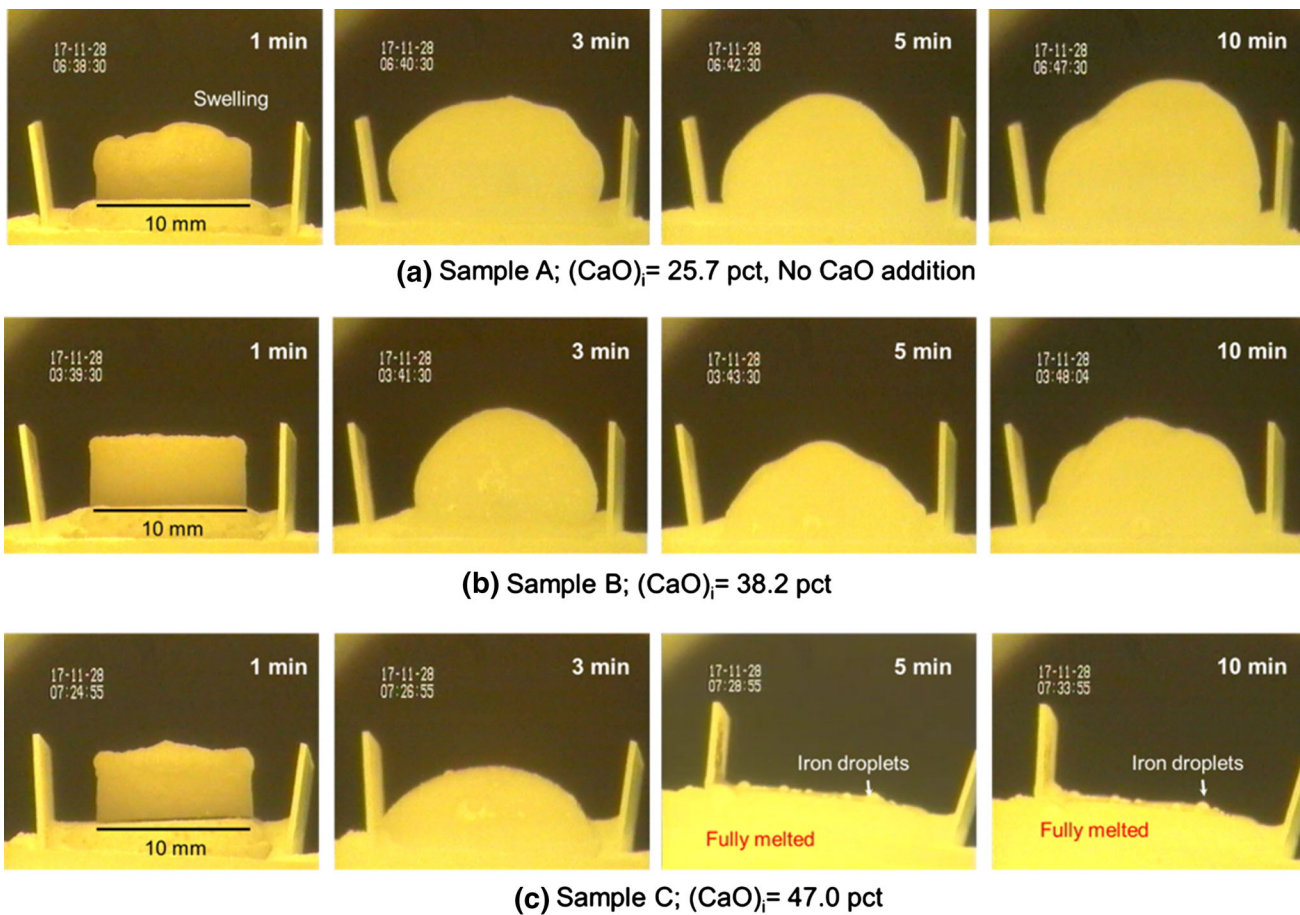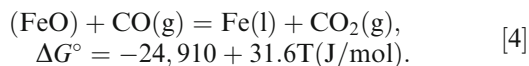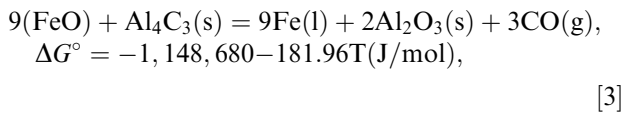

(c) Sample C; (CaO)ᵢ= 47.0 pct

Fig. 2—Shape changes of mixture pellets as a function of the initial CaO content of (*a*) 25.7 pct, (*b*) 38.2 pct, and (*c*) 47.0 pct at various reaction times at 1773 K (1500 °C).

$$9(FeO) + Al_4C_3(s) = 9Fe(l) + 2Al_2O_3(s) + 3CO(g),$$
$$\Delta G^\circ = -1,148,680 - 181.96T(J/mol),$$
[3]

$$(FeO) + CO(g) = Fe(l) + CO_2(g),$$
$$\Delta G^\circ = -24,910 + 31.6T(J/mol).$$
[4]

To confirm the governing reaction, the mass balance between consumption of FeO and production of Al_2O_3 or CO gas was estimated, as shown in Figure 4. Even though there is a slight deviation from a theoretical slope (=1/3) in production of Al_2O_3 at a given FeO consumption, the reaction stoichiometry is in good agreement with the aluminothermic reaction given in Eq. [1]. Thus, the contribution of Al_4C_3 to the reduction of FeO is much less than that of metallic Al. Similar results were found in our previous research.[24] Nevertheless, in the present study, the carbothermic reaction was readily observed because the pellet heats gradually after it enters the hot zone.

In Figure 2, the pellet height decreased with increasing initial CaO content at reaction times > 1 minute. Especially the pellet of Sample C ([CaO]$_{initial}$ = 47.0 pct) was fully melted after 5 minutes, unlike the pellets of Sample A (as-received EAF slag) and Sample B ([CaO]$_{initial}$ = 38.2 pct), indicating that slag is affected by thermophysical properties such as viscosity and surface tension. Choi and Lee[26] calculated iso-surface tension contours in the CaO-SiO$_2$-Al$_2$O$_3$ slag system at 1873 K (1600 °C) using a modified Butler's equation. According to their results, slag surface tension increases with increasing CaO content. Even though surface tension increased with increasing CaO content from Sample A (25.7 pct CaO) to Sample C (47.0 pct CaO), the latter had clearly collapsed at 5 minutes. This means that not only the melting point but also the viscosity of slag decreases with increasing CaO content.

Because the reacted slag should be a high-Al$_2$O$_3$ system owing to the aluminothermic reduction reaction as well as the properties of ABD itself, appropriate CaO fluxing can reduce the viscosity by changing the system to a calcium aluminate, which has a lower melting point. In previous research,[24] it was clearly confirmed that the
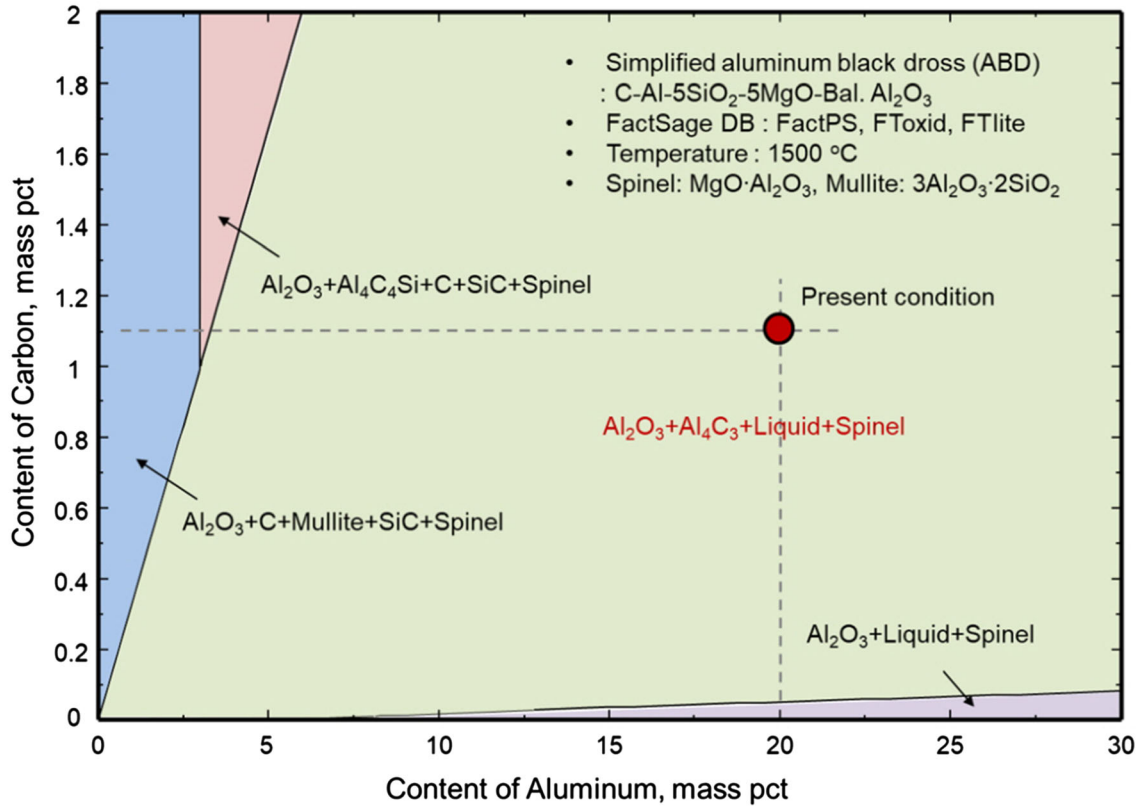
Fig. 3—Phase stability diagram of aluminum black dross (ABD) at 1773 K (1500 °C) as calculated using FactSage™ 7.3 software.
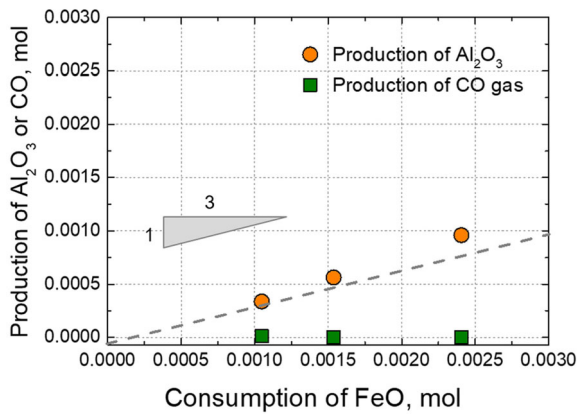

Fig. 4—Mass balance of the consumption of FeO with the production of Al_2O_3 and CO gas.

apparent viscosity decreases with increasing CaO content, meaning that the slag is highly fluid. In addition, we observed reduced iron droplets at the surface of molten slag, as shown in Figure 2(c). This is evidence of aluminothermic as well as carbothermic reduction.

The evolution of gases (CO, CO_2, and CH_4) as a function of the initial CaO content at various reaction times at 1773 K (1500 °C) is shown in Figure 5. CO and CO_2 gases evolved in the given reaction time but the CH_4 gas evolution is negligible. Namely, CO and CO_2 are the major gas products based on Eqs. [3] and [4]. In Sample A (as-received EAF slag), the trend of CO gas

production is abnormal, unlike in Sample B ($[CaO]_{initial} = 38.2$ pct) and Sample C ($[CaO]_{initial} = 47.0$ pct). In other words, it is relatively difficult to evolve CO gas to break through the slag phase owing to the high viscosity in Sample A.

To additionally evaluate the effect of the initial CaO content on the change of sample's appearance, apparent morphologies of each slag sample with side- and top-view images are shown in Figure 6. From top-view images, all pellet samples gradually spread out to empty spaces on substrate irrespective of CaO content as the reaction proceeds. It is noticeable that slag morphologies change from the cylindrical pellet to clear hemisphere-like shape with increasing initial CaO content and reaction times, except for Sample A, which is only has a distorted shape, unlike Samples B and C at 5 minutes. The distorted morphology of Sample A is well reflected in the results of the CO gas evolution tendency in Figure 5(a). From the side-view images, the sample height apparently decreased with increasing initial CaO content and reaction times. According to the change of sample morphologies by evaluating side- and top-view images, it can be indirectly understood that the melting point as well as slag viscosity decreased with increasing initial CaO content.

Figure 7 shows the vertical section of samples and the summarized features as a function of the initial CaO content and reaction times. It was confirmed that the surfaces of all samples at 1 minute are slightly swollen because of the insufficient reaction time. Thus,
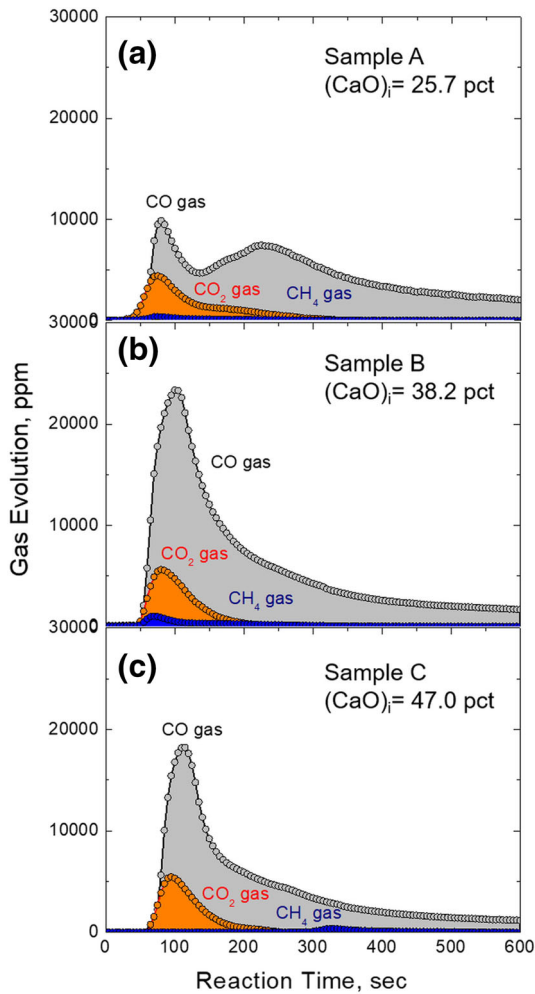
Fig. 5—Evolution of gases (CO, CO_2, and CH_4) as a function of the initial CaO content of (*a*) 25.7 pct, (*b*) 38.2 pct, and (*c*) 47.0 pct at various reaction times at 1773 K (1500 °C).

Fig. 6—Apparent morphologies with side and top views as a function of the initial CaO content of (*a*) 25.7 pct, (*b*) 38.2 pct, and (*c*) 47.0 pct at various reaction times at 1773 K (1500 °C).

undissolved lime particles in the bulk slag are observed in Samples B and C. As the reduction reaction proceeds, all samples (except for Sample A at 5 minutes) exhibited a hemisphere-like shape accompanied by melting and reactions. Note that Samples A and B containing large sizes of entrapped gas pores are more expanded than Sample C. In addition, entrapped iron droplets as a reaction product are identified in Samples A and B. In contrast, Sample C exhibits relatively gentle shape with less small pores. Moreover, iron droplets were rarely entrained in Sample C, which means that reduced iron droplets were easily separated from molten slag.

From multi-directional macroscopic observations of sample morphologies represented in Figures 2, 6, and 7 varied with the initial CaO content and reaction times, it was confirmed that CaO fluxing into EAF slag reduces slag viscosity when ABD is used as a reducing agent. However, it is necessary to consider the slag morphologies from the microscopic viewpoint to understand the reaction mechanism under the present conditions.
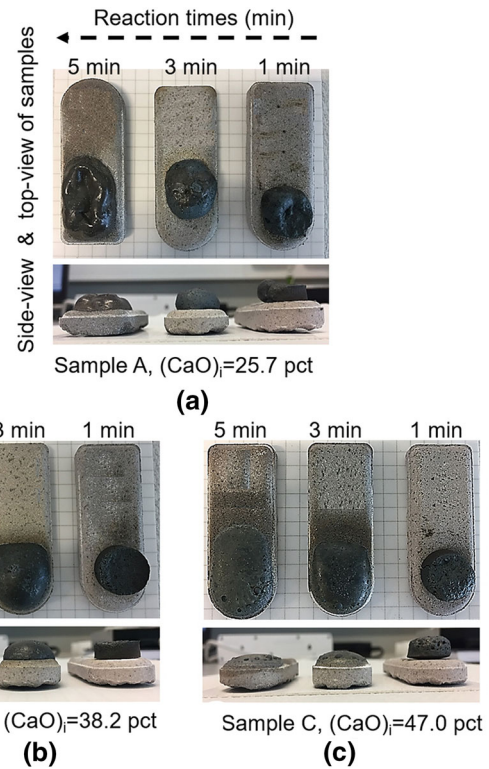
B. Microscopic Observations of Slag Morphologies at Different Initial CaO Contents and Reaction Phenomena

For clear comparison of the effects of the initial CaO content on the morphologies of slag pellets during the reaction, microscopic observations of cross sections of Sample A (25.7 pct CaO) and Sample C (47.0 pct CaO) at 5 minutes reaction time were performed, including elemental mapping by means of back-scattered electron SEM (Figures 8 and 9). Bubbles of various sizes and entrapped reduced iron particles were observed in Figure 8. Note that the formation of entrapped gas bubbles and reduced iron droplets is strongly promoted by high slag viscosity, which hinders the escape of gas bubbles and reduced iron droplets through the slag phase.

Kongkarat et al.[27] investigated the interfacial reaction between metallurgical coke and EAF slag using a sessile drop arrangement to understand carbon/slag interaction phenomena. They observed large number of small reduced iron droplets in bulk slag and at the gas/slag and slag/carbon interface from the optical microscopic image of cross-sectional slag droplets after the reaction. Furthermore, entrapped gas bubbles were also observed. Thus, even though the reducing agent used in the current study (*i.e.*, ABD) is different from that used in Kongkarat et al.' study, the observation results of the slag/carbon reaction at the interface, *i.e.*, carbothermic reduction, are in good accordance. In addition, various carbonaceous reducing agents including polymeric
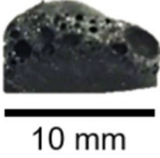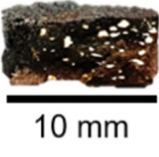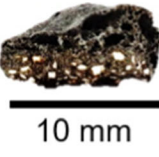
Samples	Vertical section of samples			Features
	1 min	3 min	5 min	
Sample A (CaO)$_i$= 25.7 pct	10 mm			• A number of pores • Large size of pores • Noticeable entrapped iron droplets • Highly expanded slag
Sample B (CaO)$_i$= 38.2 pct	10 mm			
Sample C (CaO)$_i$= 47.0 pct	10 mm			• Several number of pores • Small size of pores • Gentle shape of slag

Fig. 7—Vertical section of samples and its features as a function of the initial CaO content and reaction times at 1773 K (1500 °C).

waste materials were used to reduce FeO in slag, in which the dynamic interfacial reactions were comprehensively reported in the literature.[28–30]

Compared with the results for Sample A (in Figure 8), gas bubbles and reduced iron droplets were rarely observed in Sample C (in Figure 9). This is because highly fluid slag formed, facilitating the escape of gas bubbles and reduced iron droplets through the slag phase.

Large bubble holes (Figure 8) may form because of the coalescence of smaller bubbles that are unable to break through the slag phase. At this time, the pellet sample apparently expanded (swelling). When larger gas bubbles break through slag phase, the swelled pellets will instantaneously collapse (shrinking). In addition, small gas bubbles near the surface of the slag can break through the slag phase relatively easily. The gas bubbles can continuously form if the driving force for the reduction reactions that produce gas bubbles is sufficient, and the gas bubbles formed will attempt to escape the slag phase. Thus, the pellet will repeatedly expand and collapse, showing swelling-shrinking phenomena, but the rate of gas evolution gradually declines. When the slag is highly fluid, like in Sample C, these phenomena will not be aggressive.

Teasdale and Hayes[31] carried out an *in-situ* observation of the reaction interface between graphite and slag using the transmission technique. They observed large gas bubbles of 1.5 to 2.5 mm diameter in the slag phase and observed that these gas bubbles expanded and collapsed at regular intervals. In addition, metallic iron was observed to form at the graphite/slag interface. Our observations of swelling-shrinking phenomena are in good agreement with their results.

C. Effect of the Initial CaO Content on the Slag Viscosity and Thermodynamic Consideration

To quantitatively understand the shape change of the pellets, the apparent viscosity (poise) was calculated using the Einstein-Roscoe equation, and the spinel ([Mg,Fe]Al$_2$O$_4$) activity was calculated using the
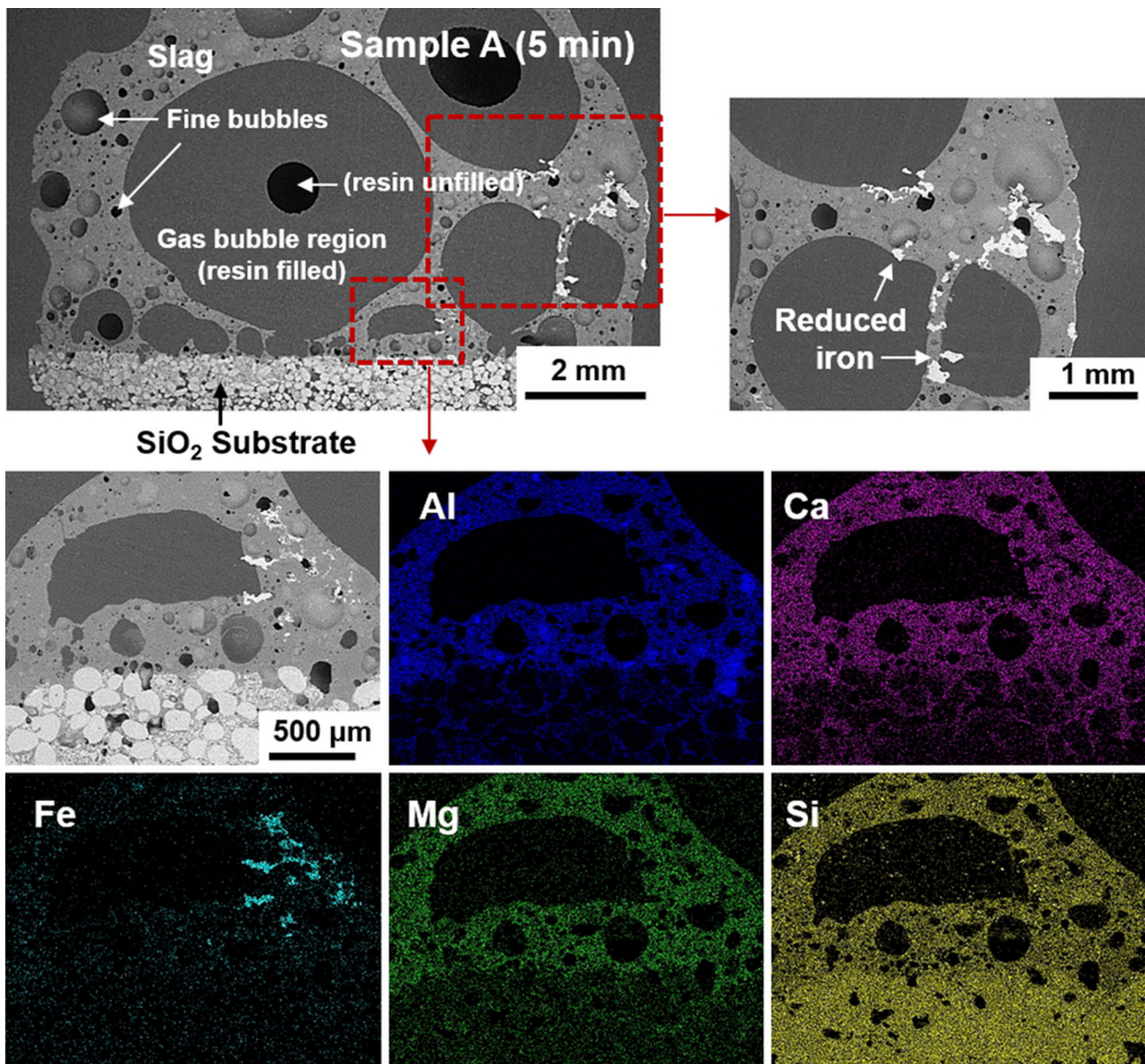
Fig. 8—SEM images and elemental maps of Sample A (25.7 pct CaO) after 5 min of heating.

FactSage™7.1 software.[32,33] We also compared the apparent viscosity with experimental results based on macroscopic observations of the specimens of various initial CaO contents in Figure 10. Although there was a clear difference in apparent viscosity between the equilibrium calculation and experimental data, both showed a declining trend with increasing initial CaO content. A discrepancy between the equilibrium calculation and experimental data possibly originates from an underestimation of the effect of the solid fraction upon the apparent viscosity. However, the effect of CaO fluxing upon the apparent viscosity in the liquid-solid coexistence region is more remarkable than in the fully liquid region. Note that the fully liquid Sample C showed good agreement with the thermodynamic interpretation for spinel activity ($a_{spinel} = 0.95$), which is lower than unity. At this point (Sample C), the apparent viscosity from

the equilibrium calculation using FactSage corresponds well to the apparent viscosity obtained from experimental data.

The precipitation of solid compounds was experimentally confirmed by X-ray diffraction (XRD) analysis of the slag Samples A to C at 5 minutes, as shown in Figure 11. The spinel ($MgO \cdot Al_2O_3$) appeared in all samples, while gehlenite ($2CaO \cdot Al_2O_3 \cdot SiO_2$) is identified in Samples B and C because of the extra CaO addition. Therefore, it is confirmed that the measured XRD patterns are qualitatively in good accordance with the computational predictions of the formation of solid compounds in the present systems.

In summary, the effect of CaO fluxing upon slag morphology was investigated during the reduction of FeO in EAF slag by ABD. It was confirmed that both aluminothermic and carbothermic reduction occurred,
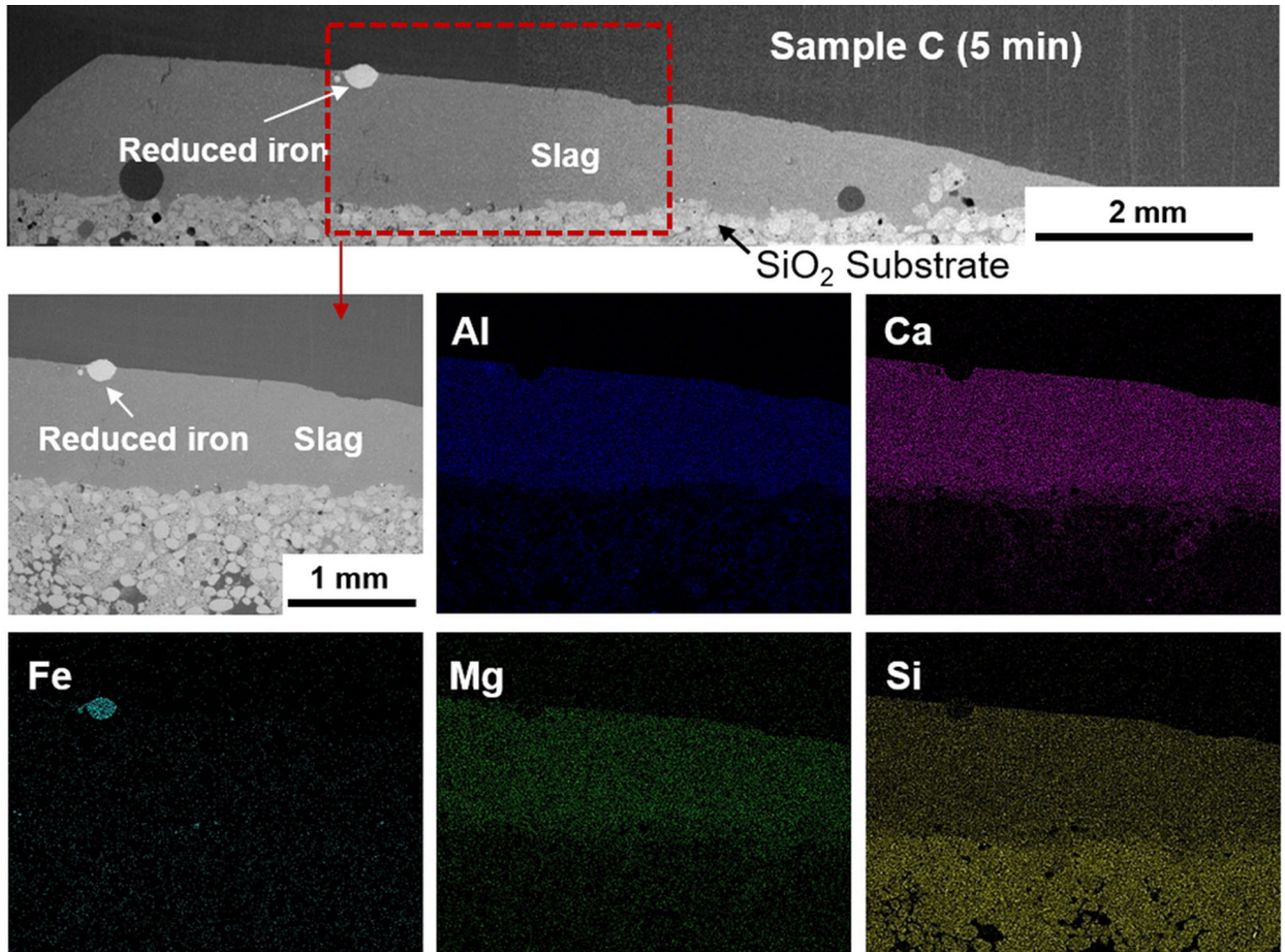
Fig. 9—SEM images and elemental maps of Sample C (47.0 pct CaO) after 5 min of heating.
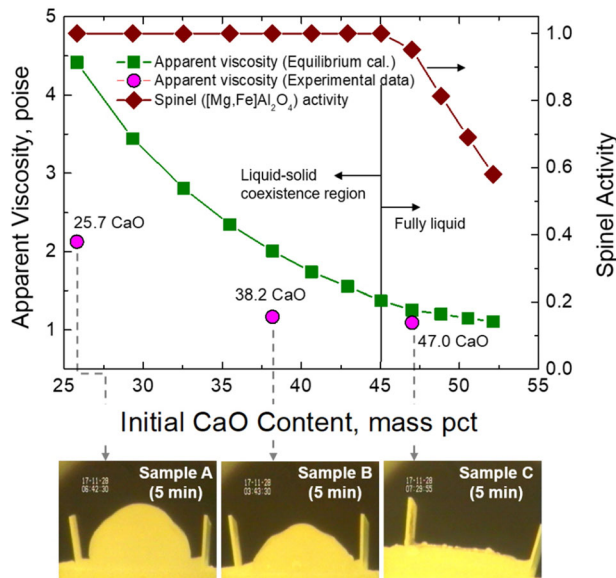

Fig. 10—Apparent viscosity and macroscopic observations for various initial CaO contents.

and thus the production of $CO(+CO_2)$ gas caused swelling-shrinking phenomena with repeated expansion and collapse of the slag pellet based on the results of macro- and microscopic observations. In addition, macroscopic observation of slag morphologies as a function of the initial CaO content is well associated with quantitative consideration of apparent viscosity as well as spinel ($[Mg,Fe]Al_2O_4$) activity. Consequently, appropriate CaO fluxing is necessary to control the composition of highly fluid slag by changing the slag from a high-alumina system to a calcium-aluminosilicate melt when utilizing ABD as a reducing agent.

IV. CONCLUSIONS

The effect of CaO fluxing on slag morphology was investigated during the reduction of FeO in electric arc furnace (EAF) slag by aluminum black dross (ABD). Our major findings of present study are as follows.

1. From the macro- and microscopic observations, by evaluating entrapped gas bubbles and reduced iron droplets related to gas evolution, apparent slag morphologies, and vertical section of slag at different initial CaO contents and reaction times, it was con-
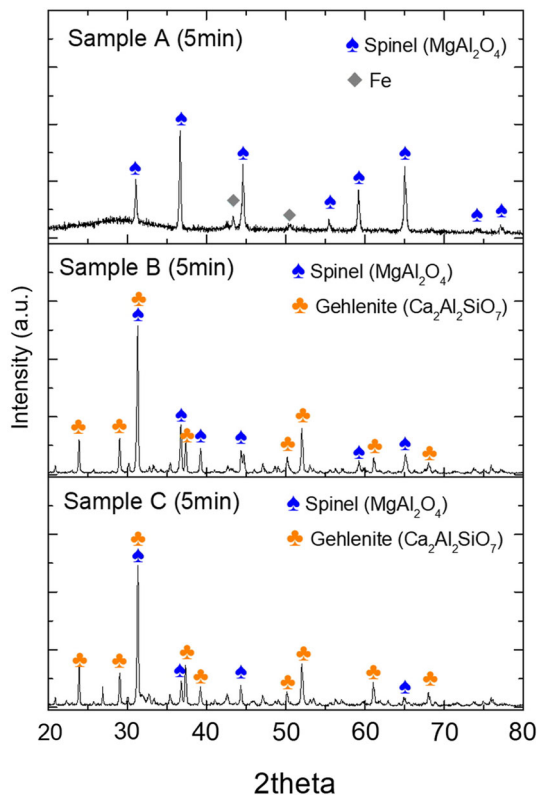
Fig. 11—XRD analysis of Sample A to C at 5 min.

firmed that both aluminothermic (dominant reaction) and carbothermic reduction (minor reaction) occurred, and thus the production of $CO(+CO_2)$ gas caused swelling-shrinking phenomena with repeated expansion and collapse of the slag pellet.

2. Macroscopic observation of slag morphologies as a function of the initial CaO content is well associated with quantitative consideration of the apparent viscosity as well as spinel ($[Mg,Fe]Al_2O_4$) activity.

3. Appropriate CaO fluxing is necessary to control the composition of highly fluid slag by changing the slag from a high-alumina system to calcium-aluminosilicate melts when utilizing ABD as a reducing agent.

4. Consequently, it can be understood that slag fluidity is a very important factor affecting the efficient recovery of valuable metals from molten EAF slag by a reduction process.

REFERENCES

1. J.Y. Hwang, X. Huang, and Z. Xu: *J. Min. Mater. Charact. Eng.*, 2006, vol. 5, pp. 47–62.
2. P.E. Tsakiridis, P. Oustadakis, and S. Agatzini-Leonardou: *J. Environ. Chem. Eng.*, 2013, vol. 1, pp. 23–32.
3. European Waste Catalogue and Hazardous Waste List, Environmental Protection Agency, Ireland, 2002. ISBN: 1-84095-083-8.
4. F.A. López, E. Sáinz, A. Formoso, and I. Alfaro: *Can. Metall. Q.*, 1994, vol. 33, pp. 29–33.
5. O. Manfredi, W. Wuth, and I. Bohlinger: *JOM*, 1997, vol. 49, pp. 48–51.
6. E. David and J. Kopac: *J. Hazard. Mater.*, 2013, vol. 261, pp. 316–24.
7. T. Hashishin, Y. Kodera, T. Yamamoto, M. Ohyanagi, and Z.A. Munir: *J. Am. Ceram. Soc.*, 2004, vol. 87, pp. 496–99.
8. M.C. Shinzato and R. Hypolito: *Waste Manag.*, 2005, vol. 25, pp. 37–46.
9. B.R. Das, B. Dash, B.C. Tripathy, I.N. Bhattacharya, and S.C. Das: *Min. Eng.*, 2007, vol. 20, pp. 252–58.
10. A. Li, H. Zhang, and H. Yang: *Ceram. Int.*, 2014, vol. 40, pp. 12585–90.
11. J.H. Heo, E.H. Jeong, C.W. Nam, K.H. Park, and J.H. Park: *Metall. Mater. Trans. B*, 2018, vol. 49B, pp. 939–43.
12. E. David and J. Kopac: *J. Hazard. Mater.*, 2012, vols. 209–210, pp. 501–09.
13. H. Shen and E. Forssberg: *Waste Manag.*, 2003, vol. 23, pp. 933–49.
14. H.N. Yoshimura, A.P. Abreu, A.L. Molisani, A.C. de Camargo, J.C.S. Portela, and N.E. Narita: *Ceram. Int.*, 2008, vol. 34, pp. 581–91.
15. E.M.M. Ewais, N.M. Khalil, M.S. Amin, Y.M.Z. Ahmed, and M.A. Barakat: *Ceram. Int.*, 2009, vol. 35, pp. 3381–88.
16. G. Bernardo, M. Marroccoli, M. Nobili, A. Telesca, and G.L. Valenti: *Resour. Conserv. Recyc.*, 2007, vol. 52, pp. 95–102.
17. L. Muhmood, S. Vitta, and D. Venkateswaran: *Cement. Conc. Res.*, 2009, vol. 39, pp. 102–09.
18. H.S. Kim, K.S. Kim, S.S. Jung, J.I. Hwang, J.S. Choi, and I. Sohn: *Waste Manag.*, 2015, vol. 41, pp. 85–93.
19. K. Mah, J.M. Toguri, and H.W. Smith: *Conserv. Recyc.*, 1986, vol. 9, pp. 325–34.
20. H. Soto and J.M. Toguri: *Conserv. Recyc.*, 1986, vol. 9, pp. 45–54.
21. M. Ueda, M. Amemiya, T. Ishikawa, and T. Ohtsuka: *J. Japan. Inst. Met.*, 1999, vol. 63, pp. 279–83.
22. A. Takeuchi, H. Hashimoto, K. Tanaka, N. Tanahashi, and K. Nakata: *J. Japan. Inst. Light Met.*, 1996, vol. 46, pp. 592–96.
23. J.H. Heo and J.H. Park: *Calphad*, 2017, vol. 58, pp. 219–28.
24. J.H. Heo and J.H. Park: *Calphad*, 2017, vol. 58, pp. 229–38.
25. E.T. Turkdogan: *Physical Chemistry of High Temperature Technology*, Academic Press, New York, 1980, pp. 1–24.
26. J.Y. Choi and H.G. Lee: *ISIJ Int.*, 2002, vol. 42, pp. 221–28.
27. S. Kongkarat, R. Khanna, P. Koshy, P. Okane, and V. Sahajwalla: *ISIJ Int.*, 2012, vol. 52, pp. 385–93.
28. U. Kumar, S. Maroufi, R. Rajaro, M. Mayyas, I. Masuri, R.K. Joshi, and V. Sahajwalla: *J. Clean. Prod.*, 2017, vol. 158, pp. 218–24.
29. J.R. Dankwah, P. Koshy, N.M. Saha-Chaudhury, P. O'Kane, C. Skidmore, D. Knights, and V. Sahajwalla: *ISIJ Int.*, 2011, vol. 51, pp. 498–507.
30. S. Maroufi, M. Mayyas, I. Mansuri, P. O'Kane, C. Skidemore, Z. Jin, A. Fontana, and V. Sahajwalla: *Metall. Mater. Trans. B*, 2017, vol. 48B, pp. 2316–23.
31. S.L. Teasdale and P.C. Hayes: *ISIJ Int.*, 2005, vol. 45, pp. 634–41.
32. R. Roscoe: *Br. J. Appl. Phys.*, 1952, vol. 3, pp. 267–69.
33. S. Wright, L. Zhang, S. Sun, and S. Jahanshahi: *Metall. Mater. Trans. B*, 2000, vol. 31B, pp. 97–104.